

Beamline 10.3.2 at ALS: a hard X-ray microprobe for environmental and materials sciences

Matthew A. Marcus,^{a*} Alastair A. MacDowell,^a Richard Celestre,^a Edward Domning,^a Keith Franck,^a Alain Manceau,^b Gregory Morrison,^a Tom Miller,^a Howard A. Padmore^a and Robert E. Sublett^a

^aAdvanced Light Source, Lawrence Berkeley National Laboratory, 1 Cyclotron Road, Berkeley CA 94720, USA, and ^bEnvironmental Geochemistry Group, LGIT, University J. Fourier and CNRS, 38041 Grenoble Cedex, France. E-mail: mamarcus@lbl.gov

Synopsis Beamline 10.3.2 at the ALS is a hard X-ray microprobe beamline specialized for environmental and materials studies. It produces a 5-17 micron spot with an energy range of 3-17 keV, with which X-ray fluorescence mapping, μ -EXAFS and μ -XRD can be done on the same sample at the same position.

Abstract This beamline, whose source is a bending magnet at ALS, is designed mostly for work on environmental problems involving heavy metal speciation and location. It offers a unique combination of X-ray fluorescence mapping, X-ray microspectroscopy, and micro X-ray diffraction. The optics allow the user to trade spot size for flux in a size range of 5-17 μ m in an energy range of 3-17 keV. The focusing is done using a Kirkpatrick-Baez mirror pair to image a variable-size virtual source onto the sample. Thus, the user can reduce the effective size of the source, thereby reducing the spot size on the sample, at the cost of flux. This decoupling from the actual source also allows for some independence from source motion. The X-ray fluorescence mapping is done with a continuously-scanning stage which avoids the time overhead incurred by step-and-repeat mapping schemes. The special features of this beamline are described, and some scientific results shown.

Keywords: X-ray instrumentation; microspectroscopy; microfluorescence; microdiffraction; powder diffraction; speciation

1. Introduction

This paper describes a beamline (10.3.2 at the Advanced Light Source) which has been optimised for environmental studies at hard X-ray energies. We will describe the scientific rationale and how that drives the design of the beamline, then the beamline design itself. Then, we will discuss the detection systems for micro X-ray Fluorescence (μ XRF), micro X-

ray Absorption Spectroscopy (μ XAS) and micro X-ray Diffraction (μ XRD). We will describe in some detail some aspects of the system integration and software. These topics are often neglected in discussions of beamlines, but are crucial for successful operation, especially by outside users. Finally, we will show some scientific results.

1.1. Scientific objectives

The continuing concern over environmental degradation and contamination has prompted a number of studies of the speciation of toxic elements in soils and plants. The rationale is that the toxicity of an element depends on its bioavailability, which in turn depends on its solubility, which depends on its chemical form. Also, intelligent design of remediation programs requires detailed chemical knowledge of how the toxic element is sequestered in the environment.

Natural materials such as soils are inhomogeneous over all length scales, down to the nanometer. It could therefore be argued that only probes with nanometer resolution could provide useful information. However, such probes only sample extremely tiny sample volumes and often cannot examine dilute species or samples in a natural state. Fortunately, many studies have shown that micron-scale studies are sufficient for many purposes because the nanometer-scale structures are grouped in micron-scale aggregates. For example, studies of soil ferromanganese nodules show composition gradients over tens of microns which correlate with regions of constant speciation of trace element speciation. Often, these trace elements are sorbed to clays or phyllosulfates, which are nanostructured materials. Although the nano-scale detail can't be seen with micron-size probes, it can be and has been inferred with a high degree of confidence. For more on this topic, including references, see Manceau, et. al. (2002a).

The field of materials science can also present us with small, inhomogeneous samples. A classic example is the combinatorial library, which consists of small patches of different materials, or a film whose composition varies continuously as a function of position. Defects in semiconductor devices may also take the form of small precipitates. Also, it is sometimes useful to orient a sample, but it may not be possible to do so over a large area, as in one of the examples discussed below.

1.2. Specifications of the beamline

What features would one want in a beamline in order to undertake such studies? First, since many of the species of interest are highly dilute, one wants to be able to maximize flux, even if a trade-off against spot size is required. Second, the beamline should be able to do X-ray fluorescence mapping, which lets one see what elements are present in the sample and

where they are, XAS (X-ray Absorption Spectroscopy) on a selected spot, and powder diffraction on the same spot. By bringing these three techniques to bear on the same sample, one can create a much clearer picture than would be possible by doing only one or two of these experiments.

Since the source is a bending magnet, we had the additional requirement of using the limited brightness in an efficient manner.

The beamline was built to the following specifications:

1. The source is a 1.27T ALS bending magnet, whose critical energy is 3keV.
2. The beam is monochromatic, with X-ray Absorption Near-Edge Spectroscopy (XANES)-grade resolution and an energy range of 3-17keV. The lower limit is determined by air absorption; the upper by the decrease in flux with energy of the bending magnet source and by the wish to get to the U L₃ edge.
3. The spot size is 5-20μm.
4. The system must do X-ray Fluorescence (XRF) mapping, followed by XAS and/or X-ray Diffraction (XRD) at a point selected with reference to the XRF map.

1.2.1. Synergy between three techniques

The three techniques, XRF, XAS and XRD, probe different aspects of the sample, and hence work together to allow a more complete analysis than any one or two of these methods could by themselves. XRF shows where the trace elements are and with which major elements they're associated. Suppose that one finds a pattern in which a trace element, say Ni, is associated with a major one, say Mn. It would be tempting to conclude that Ni is sorbed on or included in a Mn-bearing species, but such a conclusion would be unfounded. The Ni could be in a mineral which grew over a Mn-bearing species, or which was produced by the same chemical processes as the Mn-bearing species but isn't an Mn mineral itself. Therefore, an element-selective probe is needed, which is where XAS comes in. With XAS, one can study small concentrations of the element of interest and ignore the major elements.

Unfortunately, XAS doesn't provide complete information about the crystal structure of the matrix. In complex materials, XAS can only be interpreted when there is a limited list of possible species. Further, XAS gives only indirect evidence for the crystalline ordering of the host species.

XRD can be used to identify the dominant mineral species at a given location in the sample. While it is not guaranteed that this species is the host of the trace element of interest, the identification of the dominant species can help one understand the sorption behaviour of the trace element. For instance, if XAS shows the trace element incorporated in or sorbed to a mineral which XRD identifies as being a minor constituent, then one might reasonably infer

that this mineral may be a stronger sorbent for the trace element than the dominant mineral at the location being probed.

The use of a monochromatic beam for XRF mapping offers some advantages which often offset the disadvantage of having less flux than a white-beam probe. With a white probe, elastic scattering contributes to an intense background over the entire spectrum, whereas a monochromatic probe generates elastic and Compton peaks over a narrow range of energies, which can be tuned to be far away from the line of interest. When the sample is a single crystal or coarse polycrystal, Bragg diffraction can put intense, spurious peaks into the spectrum from a white source, whereas such peaks can only be part of the elastic background for a monochromatic source and may often be avoided by changing the energy. Suppose one wants to detect a small amount of an element in the presence of a large amount of another whose edge energy is higher than that of the desired element. In that case, one can place the excitation energy between the two edges and eliminate almost all of the background from the unwanted element. Finally, the energy resolution of a solid-state detector such as is usually used for this sort of work is insufficient to distinguish between many common pairs of elements such as Ba/Ti and Pb/As. However, by mapping at energies just above and just below the Pb L_3 edge, one can perform a subtraction to isolate the Pb L_α and As K_α counts separately.

1.3. Role of system integration

System integration and user interfaces are often-neglected aspects of beamline design. A poor system design can make it difficult to upgrade the beamline and to perform different measurements on the same sample at the same location. In our case, we wanted the fluorescence detector and scanning sample stage to be usable for XRF and XAS without a lot of overhead regarding the switching of modes. Thus, the XAS program can move the stage to points described by coordinates taken from XRF maps.

We will describe how multiple computers are used in a network to separate out the low-level beamline control functions from the higher-level data-taking and data-analysis processes.

In general, the sample stage and the fluorescence detector and its electronics are considered to be part of the beamline system, rather than add-ons. Having these items as permanent parts of the beamline minimises the amount of time lost in the transition between experiments.

2. Optics

The optical layout is as shown schematically in Figure 1. The source is focused at unit magnification by mirror M1 onto a set of adjustable slits which form a virtual source, which

in turn is demagnified by the rest of the optics. The light from this virtual source is collimated in the vertical direction by M2, monochromated by the two-crystal, fixed-exit monochromator, then focused to a spot by M3 (vertical focusing) and M4 (horizontal focusing). The demagnification is 20 in the horizontal and 5.6 in the vertical. All mirrors are coated with 8nm of Rh over 25nm of Pt over 5nm of Cr on Si substrates and are used at 4mrad incidence angle. The rationale for this stack is as follows: The Cr is a glue layer. Platinum is the heaviest reasonable mirror coating so gives the widest energy range for a given angle, but it has L-edges at inconvenient energies (11.56, 13.27 and 13.88keV). Rhodium is not as dense as Pt, but is dense enough to be totally reflecting at 4mrad incidence angle to energies past the Pt L-edges. Thus, an overlayer of Rh hides the Pt in the range over which Pt has edges. Finally, the Pt takes over at energies above where the Rh reflects. M1 is in its own tank with a vacuum in the 10^{-9} torr range, while M2, the monochromator, M3 and M4 are in a tank in the hutch, with a vacuum in the 10^{-7} range. When the slits are fully open, we get a source-size limited image of about 17×7 (HxV) μm FWHM (full width at half maximum). For reasons which are not clear, the minimum spot size appears to be about $5 \times 5 \mu\text{m}$. An effort is underway to acquire new mirrors for M2-M4. The resolution of the monochromator is about 2eV, depending on the energy. This resolution is sufficient to see the dip at the Cu edge in metallic Cu and the double peak in organobromines. The flux with full beam, as a function of energy, is shown in Figure 2. We now describe the various optical elements in more detail.

2.1. The virtual source

The virtual source is produced by the first mirror, which is a bent-cylindrical mirror whose short radius is such as to focus in the vertical. This orientation is sideways to the way bent-cylinder mirrors are usually used. The reason for this choice is that the source is smaller in the vertical direction than the horizontal, so we want the vertical to be less influenced by figure errors and roughness than the horizontal. In a normal, non-microfocus, beamline, this arrangement would be impractical because one wouldn't be able to accept a large amount in the horizontal. However, the focusing mirrors in the hutch can only accept a limited amount of solid angle, so that M1 can be a horizontally-deflecting toroid and need only be 0.65m long. Calculations show that the image of the source, which is about $280 \times 40 \mu\text{m}$ (FWHM), is essentially aberration-free. This image has been used by the accelerator physicists at ALS as a measure of the beam size in a sector where there is no other means of imaging the beam.

This mirror, to which we refer as M1, is bent by means of torques applied to the ends. Stainless-steel blocks are glued to the end of the mirror, and leaf springs bolted to these blocks. The other end of each leaf spring is bolted to one end of a linear stage, so that the

distance between the springs may be varied, thus causing the application of equal couples to each end of the mirror. This design is similar to a vertical deflecting mirror bender used on another hard-X-ray beamline (Hartman, et. al., 1998). The mirror is not cooled as the absorbed power is calculated to be 0.3W, leading to an estimated temperature rise of $<1^{\circ}\text{C}$.

The virtual source size is controlled by a set of roll slits, which consist of pairs of 10mm rods of polished W in a water-cooled holder. This holder rotates so that as seen by the beam, the gap between the rods can be adjusted from 0 to 2mm. There are two such pairs of rods, one for the horizontal and one for the vertical. The cross in which these slits are mounted is separated from the rest of the beamline piping by bellows and is mounted on a translation stage.

Small shifts in the source position can be accommodated by slight rotations of M1 about the vertical or transverse axes. Larger shifts, such as occur when the ring is re-surveyed, are accommodated by translations of the roll slits, in addition to rotations of M1. Since the vertical focusing of M1 depends on the incidence angle of the beam, if the source moves a large amount in the horizontal, then M1 must tilt and the virtual source also moves. Similarly, the vertical spot size is best if M1 performs no net vertical deflection, so large vertical source motions must be compensated for with both M1 and the slits. However, motions of this magnitude are rare and the normal tune-up is done just by using M1 rotation in both axes to steer the imaged beam onto the roll slits.

A PIN diode is mounted in a cross just downstream of the roll slits. When M1 tuning is required, the diode is inserted into the beam, the roll slits narrowed, and the current on the diode measured.

Machine vacuum is maintained up just before the roll slits. A water-cooled $50\mu\text{m}$ Be window separates machine vacuum from hutch vacuum. Thus, testing can be done with the in-hutch optics in air. Maintenance can be done on the focusing optics, monochromator, roll slits and monitor cross without having to bake out the whole beamline to machine-vacuum standards. This window is about 1.1m upstream of the hutch wall, 0.3m upstream of the roll slits.

2.2. Focusing and collimating optics

The optics downstream of the virtual source consist of three mirrors (M2-M4) and the monochromator. M2 collimates the beam in the vertical direction so that the monochromator can perform with good resolution. M3 takes the vertically-collimated beam from the monochromator and focuses it to the sample, and M4 focuses in the horizontal, making an image of the virtual source onto the sample.

All three mirrors are alike, 100mm long by 12mm wide by 5mm thick and made of Si. They are all coated with the same Rh-Pt-Cr stack as M1. All three mirrors in the hutch are mounted in unequal-couple benders with adjustable pitch, translation and end bending couples as described by MacDowell, et. al. (2001). The bend couples for all three of these mirrors are set off-line using a long-trace profilometer, so the pitch and translation are what get adjusted on-line. M3 and M4 have profiled widths in order to come close to the required shapes upon bending. Picomotors (trademark of New Focus) are used for the motions, with linear variable differential transformers (LVDTs) as sensors.

The working distance between the end of the mirror and the focus is about 60mm. Most of this distance is taken up by the wall of the optics box and a small ion chamber used to monitor the flux incident on the sample (I_0), leaving about 20mm of air between the ion chamber window and the sample. This distance is small enough so that He bagging is unnecessary for all but the lowest energies.

2.2.1. Beam camera

While tuning up of the mirrors can be done by means of the traditional knife-edge scan, it's much faster if one has a means of imaging the beam directly. To this end, we built a beam camera which can be inserted into the beam path at the focal plane in place of the sample. This camera consists of a cleaved plate of CdWO_4 followed by a 10x microscope objective followed by a low-light monochrome TV camera. The image scale is $0.7\mu\text{m}/\text{pixel}$ and the resolution is $\sim 2\mu\text{m}$, as seen by the sharpness of the images of dust particles when the plate is illuminated with visible light. A video capture program monitors the output of this camera and reports the FWHM in both directions and the position and brightness of the brightest pixel. This program performs frame averaging to reduce noise. It is thus relatively easy to find the optimum angles for the mirrors to produce the sharpest spot.

2.2.2. In-hutch mirrors

The M2 mirror deflects downward and is 1460mm from the virtual source. Thus, if the source size in the vertical is $40\mu\text{m}$, the vertical divergence, assuming perfect tuning, is $27\mu\text{rad}$, which is comparable to the Darwin width of the Si111 monochromator crystals and contributes 1.3eV of energy broadening at 10keV.

M3 deflects upward and focuses from infinity (collimated beam) to the sample, 260mm away from its centre. The net demagnification of the M2-M3 pair is 5.6:1.

A rough optimisation of the tilt angle of M2, and thus the vertical collimation of the beam, is done by taking XANES scans through the white line of Ta foil (L_3 edge), looking for the sharpest, highest possible line. However, this method is not precise enough to come to the

correct angle. It is important to get the vertical collimator tuned correctly because M2 and M3 are coupled. It is possible to get a sharp focus with M2 overfocusing and M3 underfocusing or vice versa. Thus, we need a method of judging when M2 is collimating. When the mirrors are tuned up correctly, a sharp image of the virtual source is formed at the sample and the monochromatic beam between the mirrors is collimated. Now, it is possible to shift the beam vertically by translating the second crystal of the monochromator so as to change the gap between the crystals. If M3 truly images from infinity, the image on the sample won't move when the beam is shifted vertically with respect to M3. Thus, the setting of M3 can be checked by moving the monochromator crystal and looking at the image on the beam camera. Another way to test the tuning is to move the roll slits by known amounts and measure the displacement of the beam. The tuning is only correct when the demagnification is 5.6:1. This latter method is not as precise as the monochromator-shift method. A final check of the resolution can be made by scanning the organobromine XANES feature in a commercial plastic such as Lexan or Plexiglas. These materials include organobromines in sufficient quantity to yield a strong Br signal.

The horizontal-focus mirror M4 is bent into an elliptical shape and deflects in the same direction as M1. It has a demagnification of 20:1 and a centre-image distance of 119mm. It is tuned up by closing down the roll slits and adjusting the tilt for best image. Small adjustments of one of the bend couples are sometimes also necessary to get the smallest spot size.

The power absorbed by the mirrors is quite small, so cooling in the usual sense is unnecessary. However, it is desirable to stabilize the temperature of the mirrors and their mounts. The mirror mounts are attached to a rail to which is attached a chill block through which temperature-controlled water passes. Since the mirrors are in vacuum, there is little thermal contact between them and the outside except for this mounting rail, so this simple system should isolate the mirrors from temperature variations in the hutch.

An illustration of the spot quality is shown in Figure 3. This Figure is a fluorescence map of a thin, patterned Ta film in which a cross of 40 μ m line-width has been etched from the centre. This test object was made according to the method of David, et. al. (2000). The curves on the top and right sides of the map are line-outs of the intensity. The curve does not go to zero in the vertical direction because there is significant scatter by the mirrors. We have replaced M2 since these data were taken and now see much less scatter. The resolution is about 5 μ m FWHM in each direction.

2.3. Monochromator

The height and width of the incident beam are determined by the desire to fill the mirrors. Thus, the monochromator must take a beam of about 400 μ m square. It must be reasonably agile, in case quick-EXAFS experiments are required in the future. The energy resolution has to be good enough to do XANES, and the energy range must cover edges from S to U L₃ (6-60° Bragg angle for Si111). It must be stable enough to run unattended overnight without retuning. The output beam must be fixed in height and especially in angle. Since the vertical focusing mirror M3 is optically like a lens distant from the sample by an amount equal to its focal length, an angular deviation from the monochromator transforms to a position shift of the beam on the sample. This monochromator is designed with a 3mm fixed offset. Because it handles a small beam with a small offset, its mechanics are quite different from the usual front-end monochromator such as one might find on a general-purpose X-ray beamline.

The monochromator is a two-crystal design using Si111 crystals. The crystals are mounted on a common shaft which provides the rotation. In addition, the second crystal translates to keep the exit beam at a constant height. The position of the first crystal is carefully chosen relative to the centre of rotation of the shaft so that the beam 'walks' as little as possible on both crystals. The geometry of the monochromator is shown in Figure 4. The 0° configuration is shown only for reference. The monochromator is shown accepting a 1mm-high beam. Since the beam is actually 0.4mm high, this design has some margin.

The crystals are simple rectangular blocks 10x10x20mm in size. This small size makes them easy to mount and to cool, and is a result of the small beam size. The reflecting face on each crystal is one of the long ones and is polished.

A servo motor driven Huber goniometer with a 180,000 count/rev Heidenhain rotary encoder drives and supports the main shaft. All cooling and wiring passes through this shaft to prevent wire drag on the mechanism as shown in Figure 5. The main shaft is sealed with a differentially pumped rotary seal system of LBNL design. Crystal 1 is water cooled and rigidly mounted. This crystal is glued with silver-filled epoxy to a copper sub-mount which is in turn attached with screws to a copper chill block. Thermal contact between the sub-mount and chill block is assured by a 0.05mm thick InGaSn eutectic layer. All copper parts that are in contact with the eutectic are nickel plated to prevent alloying. Water to the chill block is fed through the support structure for crystal 1. The joints are O-ring sealed. There are no air guards or dedicated water lines in this mechanism. Actually, the absorbed power is small enough to make cooling unnecessary; the real function of the cooling system is temperature stabilization. Crystal 2 is glued with silver-filled epoxy to an aluminium sub-mount. This sub-mount is screwed to a 1.5mm travel LBNL designed flexural stage. This stage is centred with the crystal spacing at 2.25mm. A picomotor drives against a spring to set the spacing. The

spring pushes against an LVDT (linear variable differential transformer) core, which pushes on a wobble pin that operates the flexure. The flexure position is thus measured by the LVDT. The flexure is mounted on a notch hinge assembly. This hinge controls the pitch (Bragg angle) adjustment of crystal 2. The hinge is spring loaded and driven by a picomotor with LVDT feedback. The axis of rotation for this hinge is the main shaft axis. This geometry minimizes the amount by which the crystal translates as the pitch is adjusted. This pitch mechanism mounts on an equivalent hinge mechanism for roll control. Any correction of roll on crystal 2 will result in a translation of the crystal in the same axis as the flexure. This has not been an issue, as the pitch and translation adjustments do not result in roll errors. The crystal-2 sub-mount is thermally anchored to the same cooled support structure as that for crystal 1, so both crystals are temperature-stabilized.

The completed mechanism was bench aligned with a height gage and an indicator. All flexures were set to their null points with crystal 2 in proper relation to crystal 1 for a mid-range energy. The mechanically complete mechanism is shown in Figures 5,6.

3. Monitoring

We have already described two forms of monitoring - the PIN diode after the roll slits and the beam microscope for tuning the mirrors. However, for XAS, good normalization can only be achieved if the incident beam is monitored after all the optics. Thus, a short-path ion chamber was built on the end of the optics box. A 25 μ m-thick Be window separates the optics box from the ion chamber. The path length of the ion chamber is about 20mm. At most energies, N₂ is a satisfactory fill gas, though a He/N₂ mixture must be used at the lowest energies, and Ar at the highest. The end of the ion chamber has a 6 μ m-thick aluminized-Mylar window.

4. Detection

Fluorescence is detected by a Canberra 7-element Ge detector (Ultra LEGe, 50mm² per element) running into XIA electronics (DXP2X Model T). These modules take the place of shaping amplifiers and multichannel analysers (MCAs). There are two modes of operation, single-point and mapping. In single-point mode, a pulse-height (MCA) spectrum is collected from each detector element. Counting is enabled by a gate signal from a timer board, such that counts accumulate only when the gate signal is high. The output counts are read back under software control. The single-point mode is what's used for XAS data collection as well as for inspection of the MCA spectrum at any desired location.

The other mode is mapping. In this mode, the DXP modules are pre-set with up to 16 spectral bins (regions of interest, ROIs) and access an internal memory which can be thought of as a two-dimensional array with as many rows as there are bins set. Upon receipt of a gate

pulse, counts are accumulated into the ROIs. When the next gate pulse comes in, the counts are loaded into a column of the 2D array and the ROIs cleared so counting can begin again. An address pointer is incremented so that the next set of counts are written into the next column of the data array. A start command initialises the system and a stop command ends data acquisition. Thus, when the stop command has been issued, the internal memory contains a summary of the spectra of X-rays detected during each of a number of gate pulses. The driver for the horizontal translation stage can be configured to emit the appropriate gate pulses at user-settable intervals. The result is that a line scan can be accumulated during a continuous move of the stage and read out when the stage reaches the end of the line. By repeating this action, with a motion of the vertical stage in between each line, we accumulate a two-dimensional map of the sample in up to 16 'colours' or spectral bins. The energy calibration in this mode is the same as in single-point mode, so single-point MCA spectra may be used for guidance in setting the bins.

In principle, it would have been possible to use histogramming memory to build a system in which the entire spectrum was stored at each point. However, this would have increased the required data-transfer rate 128-fold and made the task of displaying the data much more complex for both programmer and user. Also, no commercial system like XIA's exists with this functionality. Further, the large size of the data files produced by such a system would have meant that a binary format would be required for storage, with all the inconvenience and lack of portability that entails. For all these reasons, we opted for the reduced flexibility of a system which allows the collection of only 16 bins per sampling point. For most of what is done on this beamline, this mode provides sufficient flexibility.

The off-the-shelf version of the XIA software requires a TCP/IP server to be running, which mediates between commands from the host program and the DXP modules. We found that the overhead involved with TCP/IP calls was prohibitive, so the vendor provided a custom version of their software which could be called directly from LabVIEW.

The detector elements run with a peaking time of $1\mu\text{s}$, which translates into a measured dead time of $3.2\mu\text{s}/\text{element}$. This choice represents a compromise between detector speed and resolution, which is 250-300eV FWHM for MnK_{α} . It is possible to do deadtime correction accurately enough for XAS at count rates of up to about 300kHz/7 elements. A typical situation is that a sample will produce a few kHz of counts from Zn, in which we're interested, but hundreds of kHz of Fe counts. In that case, 1-5 sheets of aluminium foil make up an effective filter. If the total count rate is still too high after filtering, the detector can be translated away from the sample on a linear slide.

4.1. Data-acquisition modes

4.1.1. Single-point data collection

The single-point mode of operation has already been described with regard to the fluorescence detector. In this mode, we can also collect data from counters. For XAS work, we normalize spectra in the traditional way, by running the analogue I_0 signal into a voltage-to-frequency converter and counting the resulting pulses at the same time as we count pulses from the detector. In addition to I_0 , we can also measure the transmitted intensity in the same way, usually using a PIN diode or ion chamber as the detector. In order to keep the counting of the analogue signals synchronized with that of the detector, we use a timer board to generate pulses of programmed length, which are routed to the gate inputs of the scalers and the fluorescence detector subsystem.

4.1.2. Scanning-stage data collection (XRF)

The stage is an important element of the scanning system. It consists of an Aerotech ALS130-100 linear motor translation stage riding on an Aerotech ATS150-100 vertical translator. These translators are driven by an Aerotech DR300 driver. Both axes are encoded by Heidenhain linear encoders and have a resolution of 10nm. These stages have a translation range in excess of 50mm, so large samples can be examined. An important feature is that the horizontal stage electronics can be made to produce pulses at regular intervals of distance. These pulses are used to synchronize data collection during mapping.

In this mode of operation, the detector is gated by the stage, not by the timer board. Therefore, the detector gate input is connected to a relay which selects which source of gate pulses to use. The relay is controlled by the data-collection program, so that the appropriate source of gate pulses is always used.

The horizontal stage is always scanned in one direction during acquisition. The data from the first and last few points of each line are ignored as they are taken while the stage is accelerating or decelerating, thus leading to non-uniform dwell times. The retrace time, during which the horizontal stage is moving back to the start of the next line, is used for reading out the data from the line just taken and other housekeeping chores.

I_0 is measured at the end of each line, rather than at each point. A digital-to-analogue converter (DAC) is used for this measurement, rather than the pulse-counting arrangement used for single-point acquisition.

5. Diffraction

Diffraction data are taken using a Bruker SMART6000 CCD detector mounted on a three-axis (XZ Θ) stage. The detector may be removed when not needed and quickly re-installed.

The stage allows one to change the range of angles collected and switch between transmission and reflection modes. Lattice spacings down to 1\AA may be collected by raising the incident energy to 15keV . A clear pattern may be collected from a $0.5\mu\text{m}$ Fe foil in 1 second at this energy. At the other end of the spectrum, a clear ring has been obtained from the 1nm reflection of palygorskite clay. The usual exposure time is 10 minutes at 14keV , which provides a clear signal on poorly-crystallized or nanophase materials.

The detector software is not at present integrated with any of the other programs on the beamline.

6. Software and system integration

The smooth operation of the beamline depends on the integration of the high-level data-taking programs, the low-level code which controls the motors directly, and the data analysis programs. In this beamline, all of these types of programs reside on different computers, which talk over a network. We will now discuss how the system is integrated and the reasons behind our design choices.

6.1. The computer network

As mentioned above, there is a separation of functions between the code which controls the motors, and which is relatively standardized across beamlines, and the fully-custom code which takes the data. These functions are performed by different computers. A schematic of the computer and hardware network is shown in Figure 7.

There are three main computers on the beamline, to which we can refer as Control, Data, and Analysis. Control runs the M1, roll-slit and monochromator motors and monitors the PIN-diode and I_0 signals. It also puts out a signal which is used to route gate pulses to the detector electronics, taking them either from the stage or a timer board. Data takes the data, controlling the detector, scalars, timer and stage. Analysis is used for data analysis and doesn't interact with the hardware at all. When data are taken, the files are copied to Analysis before anything is done with them. Thus, no user action on Analysis can permanently corrupt the data.

There is yet another computer, Diffraction, which runs the diffraction camera. This machine runs as a stand-alone system. For the moment, acquisition of powder patterns is done under manual control.

In order to make the number of screens and keyboards manageable, KVM (Keyboard-Video-Mouse) switches are used to connect multiple machines to common screens.

All the programs are written in LabVIEW6.1 under Windows 2000, with a few DLLs (dynamic link libraries) written in C++. Hardware from National Instruments is extensively

used, which makes programming easier, since this vendor also provides the programming language. LabVIEWTM makes it relatively simple to write user-interface code which is easy to learn and operate.

6.2. Beamline control program

The beamline control programs comprise a main control program and a separate stand-alone application for controlling the gains on two current amplifiers. The main program shows the positions of the motors and the voltages read on a set of analogue inputs. This main panel is the access point for control of the video driver, the motor parameters, and scanning programs. Scans of a signal versus a motor position or versus two motor positions (2D scan) may be started from this screen.

The video subsystem is called from the main panel, and is used to analyse a spot seen on the screen, e.g. from the aforementioned beam camera. This program reports the beam centroid and full width at half maximum (FWHM), in X and Y directions. Any of these numbers may be considered as a signal for purposes of scanning. It is therefore possible to measure the beam parameters as a function of motor positions.

There are two classes of motor, real and derived. A derived motor consists of one or more real motors which are moved in coordination. The position of a derived motor is a function of those of the real motors comprising it. For instance, the roll slit sizes are derived motors, and are derived from the roll slit rotations. This is done because the width of the roll slit is a non-linear function of the angle between the beam and the line connecting the two tungsten rods which make up the roll slit. Similarly, the monochromator energy is derived from the monochromator angle (Bragg angle) and the monochromator second crystal translation. When the monochromator is asked to move to a given energy, this command is automatically translated into a Bragg angle and a second-crystal position and the two real motors moved to those positions. Similarly, if the system is asked for the monochromator energy, it reads the Bragg angle and converts it to energy. The data-taking program doesn't need to know how the monochromator works in order to move, query, or reset (recalibrate) it. If the monochromator mechanics were to be changed, some functions in the beamline-control program would be modified, but the data-taking programs would be unaffected. Similarly, if a command to recalibrate the monochromator is issued from any program which calls on the beamline control program, the recalibration propagates to all programs which use the monochromator. The derived motors may be scanned just as real ones can.

The beamline control program is a TCP/IP server which accepts commands from other programs. These commands include requests to move a motor, read its position and status, reset its position and read off the values from a bank of analogue-to-digital converters (ADCs). These ADCs are used for monitoring the PIN diode after the roll slits, I_0 and

transmitted-beam signals. Thus, it is possible to take a simple XAS scan using the beamline-control program, though the XAS data-taking program is much nicer to use for this purpose.

The positions of all the motors are stored in a daily log file which is updated every 10 seconds. These log files are grouped into a directory for each month. Each of these directories is grouped into a directory for the year. This structure is automatically maintained. Thus, if something happens so that any motor ‘forgets’ where it is, it is often possible to restore it to an appropriate state. Also, when a scan is run, the beamline control program generates a data file containing all the signals and motor positions.

The DACs and the digital signal used for switching the gate pulses are controlled by the Control computer. This computer samples the DACs continuously at a 2kHz rate, reporting an average of the last 200 samples taken when the Data computer asks for it. The gate-switching signal is managed by the same server which moves the motors. The TCP/IP commands for switching and reading this signal are identical in form to commands used for motors. Thus, there is a unified interface for control functions. This framework makes it easy to add new functions to the Control computer and to call them from Data.

The beamline-control program also has sub-programs for plotting a DAC signal versus the positions of one or two motors which are scanned over specified ranges. This option is used for tuning and diagnostic purposes. Another useful sub-program is the video driver, which is used with the beam microscope. This driver is a program which can run in the background and take data from a video input, reporting on the intensity, position and FWHM of a beam spot. These quantities may be plotted versus motor position in the same way as one of the DAC signals can be plotted. There is also an interface screen which may be opened, which allows one to look at the video image, cuts through the centroid of the spot, and the values of the centroid position, brightest pixel intensity, and FWHM in X and Y directions. This sort of live video monitoring makes tuning up the mirrors much easier than the traditional method of knife-edge scanning. When the video input is not being used to inspect the beam, it is often used to capture and save an image of the sample. This capability is useful for reminding oneself of where on the sample the data were taken.

6.3. Data-taking programs

Now we will describe the main data-taking programs and a little about the data-analysis programs on the Analysis computer.

The data-taking programs store their results in ASCII files of simple structure. A data file consists of a header containing information about the conditions under which the data were taken plus a user-specified title, followed by a data block. This simple format allows programs other than those written for the beamline to read the files. Filenames have numeric

suffixes which are automatically incremented on each scan, and can be manually set when editing the parameters of a scan.

Both main programs attempt to detect beam dumps and do something intelligent when they occur. If I_0 falls below a user-defined threshold, the programs consider that the beam has dumped. The fluorescence map program will keep re-acquiring data on the same scan line until the beam comes back. The normalization of I_0 is good enough so that the resulting image is almost seamless. Since EXAFS scans can't be so easily stopped and restarted, the current scan is saved and the program waits for the beam to return. When the beam comes back, the program starts a new scan with a filename bearing an incremented scan number suffix. This feature allows unattended data gathering.

6.3.1. X-ray fluorescence mapping

An XRF map is essentially a three-dimensional array whose indices are pixel number in X, pixel number in Y, and energy-bin number. Another way to think of it is as a multi-spectral image of the sample, taken in the 'light' of various elements. The purpose of the XRF program is to make it easy to collect such an array of data, inspect it in real time, and save it to a file for later processing.

A sample screen from this program is shown in Figure 8. The bank of controls labelled Region of Interest Settings is for defining the energy ranges for the up to 16 bins collected at each point. The user can give each bin a name, which is stored in the data-file header but has no effect otherwise. The user may change these Regions of Interest (ROIs) until a scan starts. At that point, the controls are greyed out because it would make no sense to change these ROIs in mid-scan.

Next to these controls is a column of buttons of which one is bright at any time. This button selects which ROI is imaged on the display to the right. This display may be switched while a scan is in progress. The scales of the display are automatically adjusted to keep the same scale in the X and Y directions so that a circular feature on the sample always looks circular and not elliptical.

The display is a monochrome (grey-scale) intensity display, so that points with large numbers of counts in the selected bin show up bright. The display may be colorized to suit, so that when Cu is imaged, bright areas are green, while an image in Ca might be red. We find that having the display appear in different colours for each element makes it easier to remember which element's signal is being displayed at the moment.

The cursor may be used to designate a point on the image. If a scan is not running, the stage may be sent to that point. Thus, a spot at which to collect XAS or XRD may be selected without having to write down coordinates. The cursor may also be used to designate start and

end points for a new map. Thus, one may take a coarse map with large pixels and a big, intense beam, then zoom in, cut down the size of the beam spot by closing the roll slits, then take a zoomed-in image of a selected area.

6.3.2. XAS data-collection

A sample screen from this program is shown in Figure 9. There are controls for obvious functions such as starting and stopping a scan, as well as indicators for the current energy and stage position. The upper of the two graphs on the right is the familiar EXAFS data plot. The lower one shows I_0 , but processed to make small variations such as monochromator glitches more visible. The processing consists of fitting a cubic polynomial through the data, dividing by that polynomial, and taking the natural log of the result. Thus, a dip which goes down to -0.10 represents a 10% intensity drop.

The banks of buttons to the left of the main graph select what combination of scalers to plot. ROIs in the fluorescence detector may be treated as scalers. Usually, the scalers are (top to bottom) I_0 , transmission (if used), fluorescence and total counts into the detector. The latter is used for deadtime correction in analysis. One may specify that the quantity plotted is the sum of any set of scalers, the ratio of such a sum to any other sum, or the natural log of a sum or ratio. These possibilities cover almost anything one might want to plot. The plot may be changed at any time, during or after data collection.

Normally, we take the sum of counts from all seven detector elements to be one of the scalers, but if desired, one may specify that the counts from each element be stored and plotted separately. This capability is useful when the sample is a single crystal and throws strong Bragg reflections into the detector, or when one is using the grazing-exit method for measuring the EXAFS of a concentrated sample.

The plot screen displayed in Figure 9 is one page of a tabbed control. Clicking on the tab reveals a page containing buttons for moving and resetting the monochromator, taking offsets, measuring the signal, and defining the scan.

A set of scans may be taken at one point on the sample, or a set of points may be defined. In the latter case, the program will automatically cycle through the points. This feature is handy for unattended data collection on a sample with several interesting spots. Also, some samples are vulnerable to radiation damage, so it is useful to move from place to place between scans, rather than exposing a single point to a large dose.

The EXAFS program has a number of small user-interface 'frills', which together make the program relatively pleasant to use. To give one example, anywhere the user must specify an energy, a form like 'aul3-50', meaning 50eV below the Au L_3 -edge, may be used instead of a number.

The program is organised internally as a finite-state machine, which is a good way to design a program with complex sequences of actions. For instance, there are transition rules which specify what happens in each state when a beam dump is detected. This architecture makes it relatively simple to add new functions or contingencies.

6.4. Data analysis programs

We provide a suite of small, specialized applications, rather than one large, integrated program such as WinXAS. This style eases maintenance and allows the user interfaces to be optimized for the task at hand. Also, new programs may be added without the risk of disrupting or introducing bugs into older, functioning code.

6.4.1. X-ray fluorescence

Figure 10 shows a screen-shot from the main XRF editor program. The large plot is a map of the signal from a selected element, in this case Mn, normalized to I_0 and dwell time. Controls allow the user to modify the tone curve of the display and to select which element is displayed. Buttons give access to other functions, for instance tricolour mapping. In this screen (not shown), the user can select 1-3 elements to be represented as red, green or blue. Picking the same element for each colour results in a grey-scale plot. The image may be inverted for a negative contrast, saved as a bitmap or printed. The black and white levels may be adjusted for each colour. All the tricolour maps and several of the grey-scale maps in the review by Manceau, et. al. (2002a) were produced by this part of the XRF editor.

Another button on the main panel gives access to the correlation and scatterplot screens. These allow one to examine the association between one element and another. The scatterplot shows the count for one element plotted against the counts for another, with each pixel contributing a point in the plot. It is possible to select a region on the scatterplot and use it as a mask such that the image in the main screen is blanked out except for pixels which fall within the selected region. This procedure can be useful for isolating chemically-different regions in the sample.

The correlation, scatterplot and masking functions are described and illustrated in the Manceau, et. al. review, so will not be discussed further here.

In addition to the main program, there are several auxiliary programs used for specialized functions. For instance, one of these corrects for the deadtime of the fluorescence detector, if a spectral bin corresponding to all energies has been recorded. Another subtracts the normalized counts in one map from those in another. This program is commonly used for isolating the contributions of two elements whose fluorescence lines overlap to within the resolution of the detector. For instance, as discussed in Section 1.2.1, Pb may be detected in the presence of As by making maps at energies just above and just below the Pb L_3 edge and

taking the difference. The resulting difference map has only one spectral bin of significance, that for Pb/As. However, another program may be used to insert the page of data corresponding to this bin into the map taken below the Pb edge. Thus, the inserted page represents the Pb spectral bin, and the Pb/As bin of the below-edge map represents the amount of As.

6.4.2. XAS

The XAS data files from the Data machine contain the counts from all scalers, including I_0 , the energies, and the count time for each point. This level of detail is needed for proper averaging of scans and for deadtime correction. However, most other functions require a simple 2-column form representing the signal versus the incident energy.

The EXAFS Data Editor is the first program used to analyse a set of raw data and is the interface between full-information (all columns, as above) and 2-column formats. This program provides the usual functions of deglitching, jump cancellation, averaging, energy calibration adjustment and deadtime correction which might be found in any full-featured EXAFS analysis package.

A sample screen from this program is shown in Figure 11. There is a control for choosing what is to be plotted which works exactly as does the one in the data-taking program. One can switch between plotting the normalized fluorescence (as shown) and I_0 so it becomes easy to see if a feature seen in the spectrum also shows up in I_0 and hence may be a non-normalized glitch and not real EXAFS. There is an additional button which causes the plot to display the total time/point of the spectrum; this is handy for deciding how many more scans are required for good data quality.

The data file header includes beamline-specific information such as the stage position and the roll-slit settings. This information is displayed so that the user can reconstruct the details of the data acquisition, and is the only element of the data file which is truly specific to the beamline.

Once the data have been deadtime corrected, averaged, de-glitched, and pruned to the user's satisfaction, it may be written either as a full-information file, including all scalers and count times suitable for further processing by the Editor, or as a two-column (signal vs. energy) file ready for the other programs. These other programs perform the standard XAS analysis functions such as conversion to k-space and fitting. Both the full-information and two-column files are easy to read into other packages such as WinXAS.

7. Examples of scientific results

In this section, we summarize three examples of scientific research which have been done on this beamline. Two of these are related to environmental issues, as that area is the one for which the beamline was intended, while the third is an example of materials science.

7.1. Speciation of Ni in a soil

This work was published by Manceau, et. al. (2001), so will be described only in broad outlines.

Soils often contain ferromanganese nodules, which are mm-size, sub-round concretions rich in nanocrystalline Fe- and Mn oxides. These nodules are thought to be the result of fluctuating redox chemistry, which results in the deposition of layers of Fe and Mn. These oxides have very large surface areas, so can sorb large quantities of trace minerals. It is commonly found that trace elements are enriched in these nodules relative to the surrounding soil.

In this work, the environment of Ni was investigated by means of XRF, XAS and XRD. The XRD was done at another beamline, 7.3.3, which has a unique diffraction mapping capability not yet available on 10.3.2, but XAS was done at 10.3.2. XRF mapping was done at both beamlines, in order to establish a correspondence between points probed by XRD and XAS. The samples consisted of thin sections of nodules fixed in resin, so the nodules were seen in cross-section.

It was found that the distribution of Ni, seen by XRF, matched that of lithiophorite, as seen by XRD mapping. These distributions, for one nodule, are shown in Figure 12. This mineral is a layered compound consisting of alternating MnO_2 and $\text{Al}(\text{OH})_3$ layers, with alkali or alkali earth ions between the layers. The obvious inference is that Ni is sorbed to this mineral, being included in the structure or attached to the layers or the layer edges. However, it cannot be assumed that an association between an element and a mineral implies that the element is incorporated in that mineral. For example, the Ni could be part of a phase which was deposited on or formed under the same conditions as lithiophorite.

EXAFS was done at the Ni-K edge, at a number of locations on the nodules. The EXAFS patterns were everywhere the same, and were different from that of synthetic Ni-sorbed lithiophorite. Analysis of the EXAFS and comparison with Mn-edge EXAFS showed that the Ni was indeed incorporated into the lithiophorite structure, but substituting in the Mn layers. The laboratory reference had Ni in the Al layers instead. Representative EXAFS patterns for the sample and reference are shown in Figure 13.

This example shows the usefulness of applying the three techniques, XRF, XAS, XRD, together on one sample. While 10.3.2 can't yet do XRD mapping, it can do powder patterns at single points of interest.

7.2. Forms of Zn accumulation in a plant

Our next example is also from the published literature, from Sarret, et. al (2002). It concerns the storage of Zn in a hyperaccumulating plant, *Aribidopsis halleri*. High levels of Zn are toxic to most plants. If soil is contaminated with Zn, a very common pollutant, then plants won't grow well in it unless some treatment is applied to reduce the bioavailability of the Zn. One of the many ways being tried is phytostabilization, in which plants which can grow at high Zn concentrations pick up the metal and store it in a form which is insoluble, hence less harmful to other organisms than the original form.

It was known that *A. halleri* could store large amounts of Zn, but what was not known was where the Zn was put and in what form. X-ray diffraction revealed nothing because the Zn was not in a well-crystallized form. XRF mapping showed Zn in the leaves, roots and especially the trichomes (hairs) on the leaves. Such a map is shown in Figure 14, along with EXAFS spectra from specific areas of the plant. It was found that there was a uniform background of Zn in the leaves and roots, but the trichomes showed enhanced Zn concentrations, especially in small collars around their bases. The EXAFS spectra showed that the Zn was stored in different forms, depending on where it was in the plant.

7.3. Structural anisotropy of oriented nanoclusters

This work-in-progress, carried out in collaboration with D. Michiko Aruguete, Liang-shi Li, and A. P. Alivisatos, involves using polarized EXAFS to look at the structural anisotropy of CdSe nano-rods. These rods form a nematic liquid crystal which is oriented over small (<100µm) domains. Thus, a micro-beam is required to probe an area which is homogeneously oriented. We have done Se K-edge EXAFS with the rods oriented at various angles to the polarization of the beam. In order to find a domain oriented as desired, we take diffraction patterns, an example of which is shown in Figure 15. The sharp arc is the basal (002) reflection of the wurzite structure. That it's an arc instead of a continuous ring demonstrates the orientational ordering. The other arcs are fuzzy because their diffraction wave-vectors are not along the long axis, so there are a limited number of diffracting planes in those directions.

EXAFS data taken in several different orientations are shown in Figure 16. In order to accentuate the difference between the two orientations, we have subtracted off the oscillations corresponding to the first shell, leaving the second and higher shells. We see that there is an effect of orientation, whose magnitude agrees roughly with a simple model of the rod as being

bounded by a cylindrical surface without faceting. Thus, this preliminary result demonstrates that we can use polarized EXAFS, in combination with spontaneous orientational ordering, to probe the surface structure of these particles.

8. Future developments

We intend to implement scanning XRD, which will allow for mineral mapping as in Manceau, et. al. (2002b). Also, we plan to move the beamline from its present bending magnet source to one of the new 5T superbends (critical energy = 12keV) which have recently become available at the ALS (Robin, et al., 2002; Tamura&Robinson, 2002). This new source will provide more flux in the 8-20keV range allowing useful experiments on dilute samples of the important contaminants U and Pb.

9. Summary and conclusions

Beamline 10.3.2 is a facility in which three micro-scale techniques, μ XRF, μ XAS, and μ XRD, are brought together in a way which is optimized for certain kinds of environmental research. Although the beamline was designed with a particular type of experiment in mind, it is versatile enough to be used for many other experiments not originally anticipated. A unique combination of X-ray optical hardware, detectors, software and system integration makes it possible to do experiments which can be done in few other places.

Figure 1 The overall layout of the beamline. Details are as described in the text.

Figure 2 The flux, in photons/second, of monochromatic beam at full spot size, plotted as a function of energy. Edges of Cl, Fe, Rh and Pt are visible.

Figure 3 A map of a Ta-film test object in which a cross pattern has been etched out. The lines of the cross are 40 μ m wide. The curves above and to the right of the image are line profiles showing the resolution. The ticks on the axes are 20 μ m apart.

Figure 4 The geometry of the monochromator, showing Bragg angles of 0° (reference only), 6° and 60°. A 1mm-high beam is shown incident from the left. All dimensions shown are in millimetres.

Figure 5 View from the air side of the monochromator, showing the encoder (large, annular object with radial grooves), the motor/gear reducer combination, and the mounting flange. The picomotor which adjusts the crystal translation is visible at the top.

Figure 6 View of the monochromator from the vacuum side. The beam enters from the left as in Figure 4. The monochromator is set for 0° Bragg angle, as in Figure 4a. The translation motor is visible at the top, and the pitch motor at the left. The grey blocks are the crystals, and the square aluminium assembly surrounding them is the flexure device which moves the second crystal without

tilting it. The monochromator is shown mounted on a temporary scaffold rather than on the beamline, which is why the O-ring groove is visible at the top.

Figure 7 The system organization, including the computers, stage, and counting hardware. Solid lines show the flow of data, dotted lines represent control signals, thick solid lines indicate commands from the computers, and dashed lines represent detector signals. The square-wave symbols indicate the origins of detector gate pulses.

Figure 8 A sample screen from the XRF mapping program. The As channel is shown, and gamma is set to a value less than 1 so as to show the dimmer areas, which have 1/10th as much As as the bright area flagged by the crosshairs.

Figure 9 A sample screen from the XAS program, taken during a scan at the As K-edge. The Operations tab, now hidden behind the Plots tab, contains controls for such things as moving the monochromator and editing the scan parameters. The data are plotted as fluorescence (third scaler) divided by I_0 (first scaler).

Figure 10 Screen shot from the XRF Editor program.

Figure 11 Screen shot from the EXAFS Data Editor program. As in Figure 6, the data are plotted in normalized fluorescence. The controls for deadtime correction are visible on the left. The data shown are the average of 14 scans. The header of the last-read file is shown under the data graph.

Figure 12 Distributions of Ni, Zn, Mn and Fe in a soil nodule are shown in the upper row. The corresponding distributions of goethite, birnessite, phyllosilicate and lithiophorite are shown in the bottom row. All distributions are plotted in negative-contrast greyscale so that high concentrations are shown as dark areas. We see that the distribution of Ni matches that of lithiophorite and doesn't match those of the other minerals.

Figure 13 EXAFS patterns for Ni in the soil nodule for which the elemental and mineralogical distributions are plotted in Figure 11, and for the synthetic reference. Panel a) shows the Ni-edge EXAFS, panel b) its Fourier transform, and panel c) the Fourier transform of the Ni- and Mn-edge EXAFS. (Taken from Manceau, et. al. (200b))

Figure 14 Upper panel: XRF maps of Ca, Mn and Zn in leaves of *A. halleri* plants showing concentrations of Zn in "collars" around the trichome bases and Ca in the tips. Lower panel: the Zn micro-EXAFS spectra from a trichome, the body of a leaf, and a root.

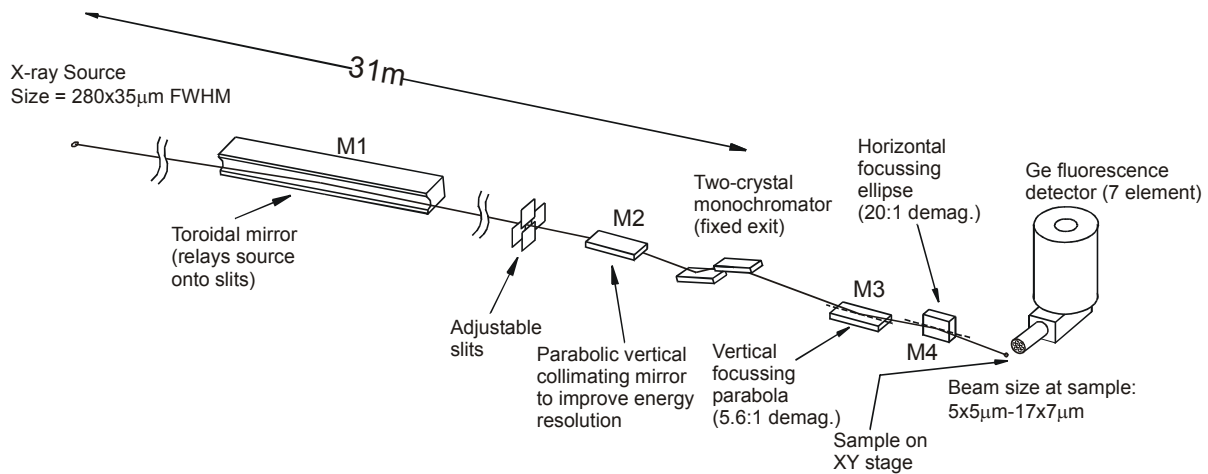
Figure 15 Diffraction from oriented nano-rods of wurzite-structure CdSe. The sharp, intense reflection is the (002), which shows the effect of orientational ordering. The dark shape is a beamstop.

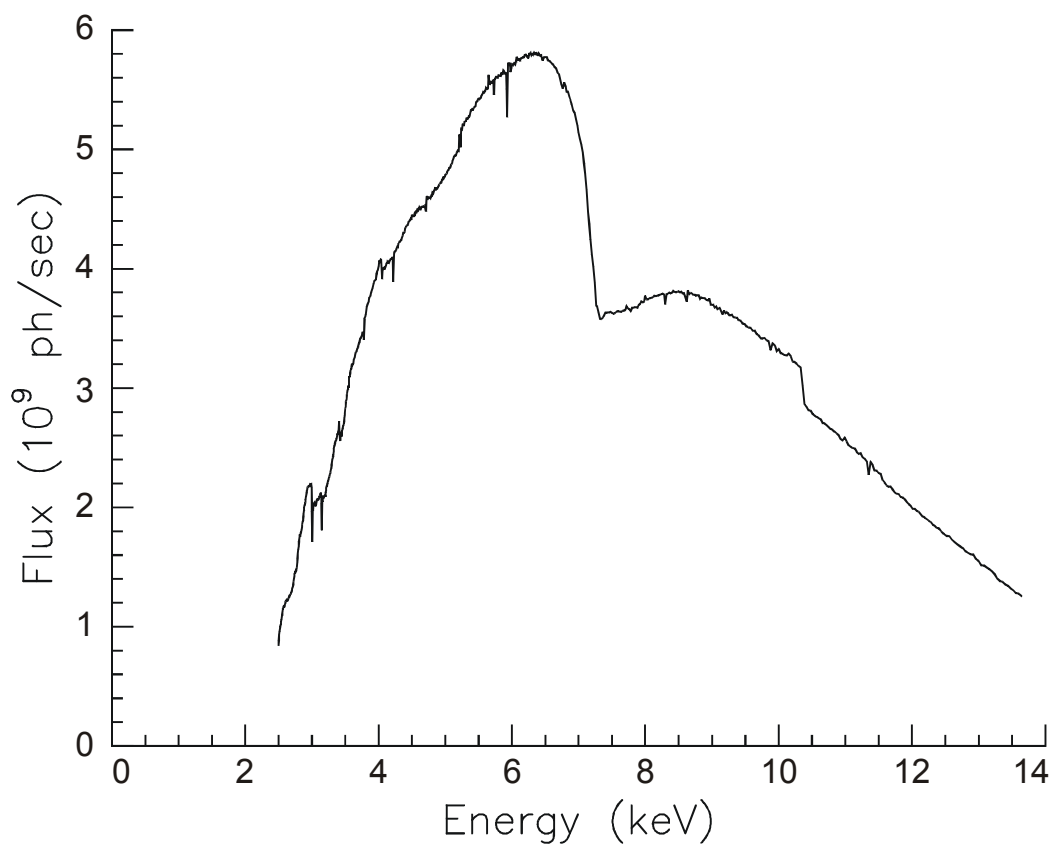
Figure 16 Se K-edge EXAFS from CdSe nano-rods oriented at several angles to the polarization. The first shell (Se-Cd) has been subtracted from each spectrum to highlight the higher shells. The angles are 15° (thick line), 33° (long dashes), 48° (thin line) and 61° (short dashes).

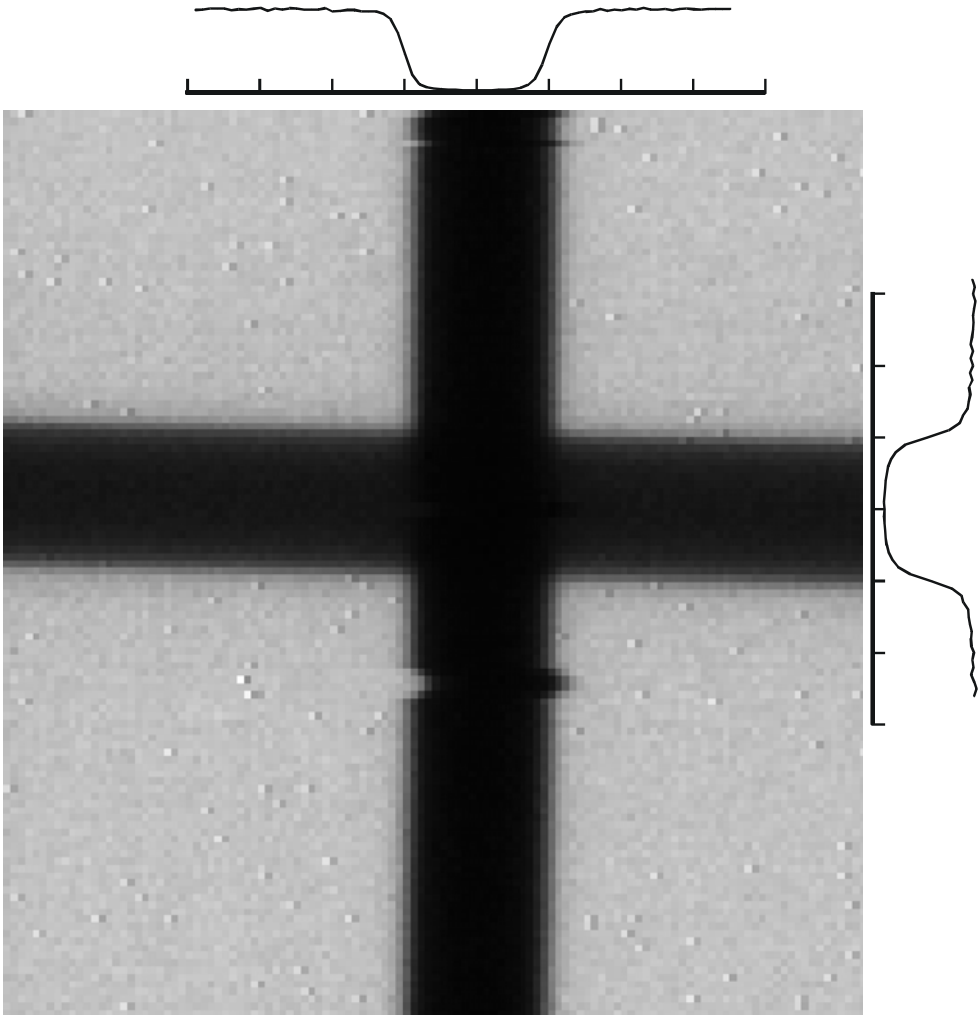
Acknowledgements The Advanced Light Source is supported by the Director, Office of Science, Office of Basic Energy Sciences, Materials Sciences Division, of the US Department of Energy under Contract No. DE-AC03-76SF00098 at Lawrence Berkeley National Laboratory. The Ta-film test object was lent to us by Christian David and Daniel Grolimund of the Paul Scherrer Institute.

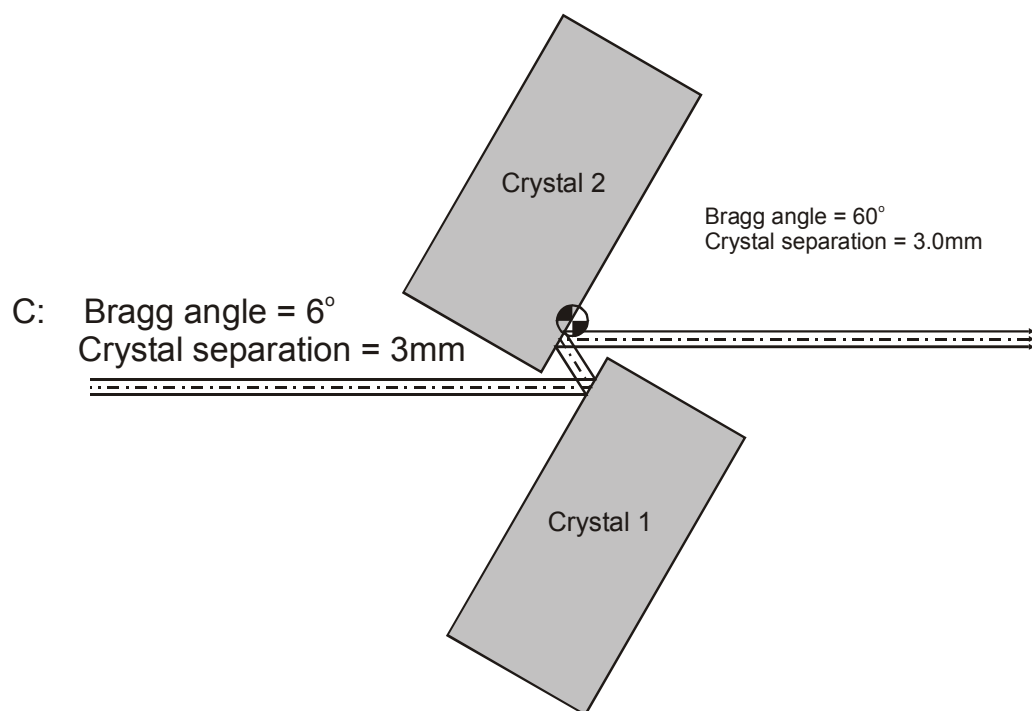
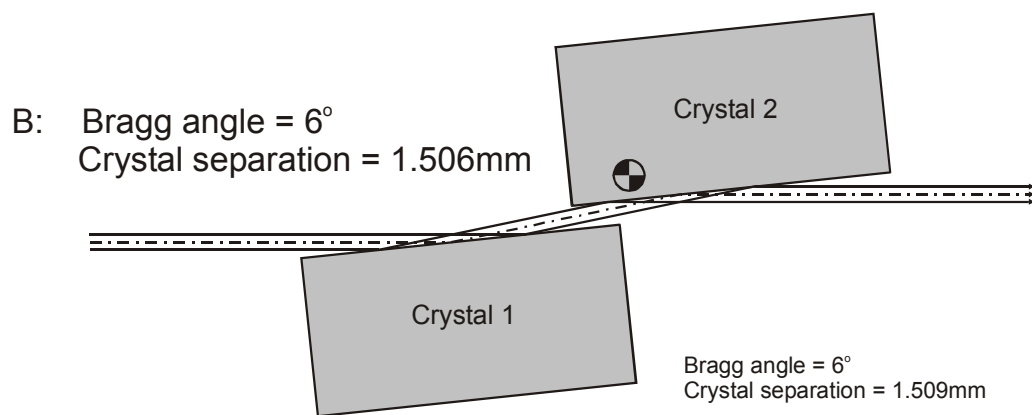
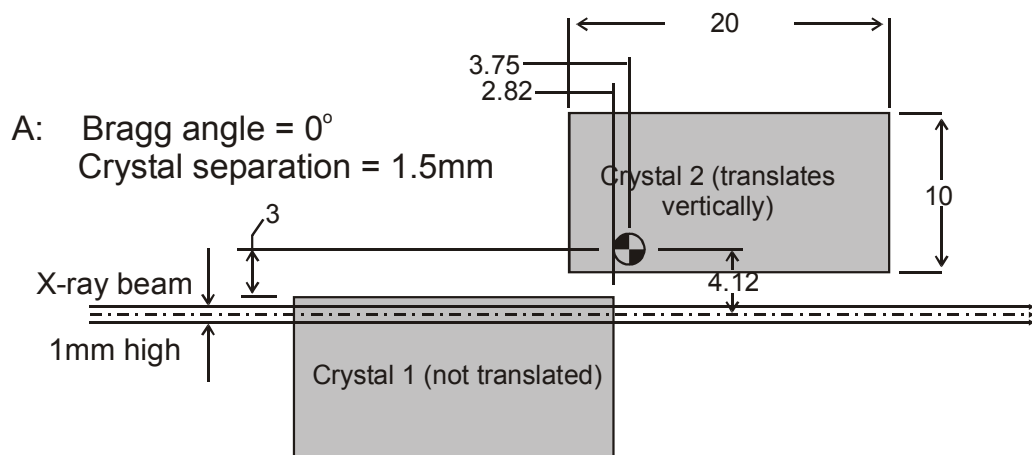
References

- David, C., Musil, C., Souvorov, A., Kaulich, B. (2000), in Proc. Sixth International Conference on X-ray Microscopy, Meyer-Ilse, W., Warwick, T., Attwood, D., Eds., American Institute of Physics.
- Hartman, N.D., Heimann, P.A., MacDowell, A.A., Franck, K.D., Grieshop, A.P., Irick, S.C., Padmore, H.A. (1998). presented at SPIE meeting held in San Diego July 19-24 1998. SPIE. **3447**, 40-51.
- Li, L. S., Walda, J., Manna, L., Alivisatos, A.P. (2002). *Nanoletters* **2**, 557-560.
- MacDowell, A.A., Celestre, R.S., Tamura, N., Spolenak, R., Valek, B., Brown, W.L., Bravman, J.C., Padmore, H.A., Batterman, B.W., Patel, J.P. (2001). *Nucl. Instrum. and Methods A*. **467-468**, 936-943.
- Manceau, A., Marcus, M. A., Tamura, N. (2002a). *Reviews in Mineralogy and Geochemistry* **49**, 341-428.
- Manceau, A., Tamura, N., Marcus, M.A., MacDowell, A.A., Celestre, R.S., Sublett, R.E., Sposito, G., Padmore, H.A. (2002b). *Amer. Mineralogist* **87**, 1494-1499.
- Sarret G, Saumitou-Laprade P., Bert V., Proux O., Hazemann J.L., Traverse A., Marcus M.A., Manceau A (2002). *Plant Physiology*, **130**, 1815-1826.
- Robin, D., Benjegerdes, R., Biocca, A., Bish, P., Brown, W., Calais, D., Chin, M., Corradi, C., Coulomb, D., De Vries, J., DeMarco, R., Fahmie, M., Geyer, A., Harkins, J., Henderson, T., Hinkson, J., Hoyer, E., Hull, D., Jacobson, S., Krupnick, J., Marks, S., McDonald, J., Mollinari, P., Mueller, R., Nadolski, L., Nishimura, K., Ottens, F., Paterson, J.A., Pipersky, P., Ritchie, A., Rossi, S., Salvant, B., Schlueter, R., Schwartz, A., Spring, J., Steier, C., Taylor, C., Thur, W., Timossi, C., Wandesforde, J. & Zbasnik, J. (2002) To be published in the proceedings of the 2002 European Particle Accelerator Conference.
- Tamura, L. & Robinson, A. (2002). *Synchrotron Radiation News*, **15**, 30-34.

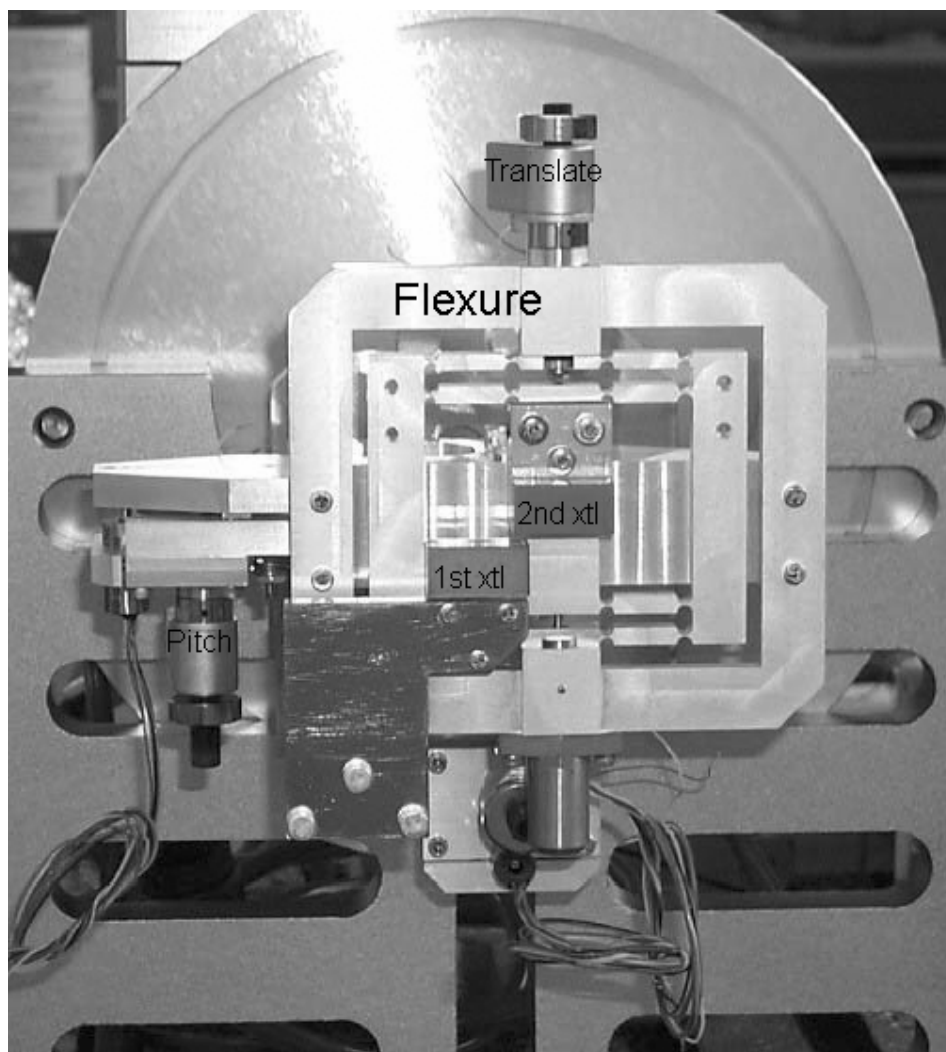


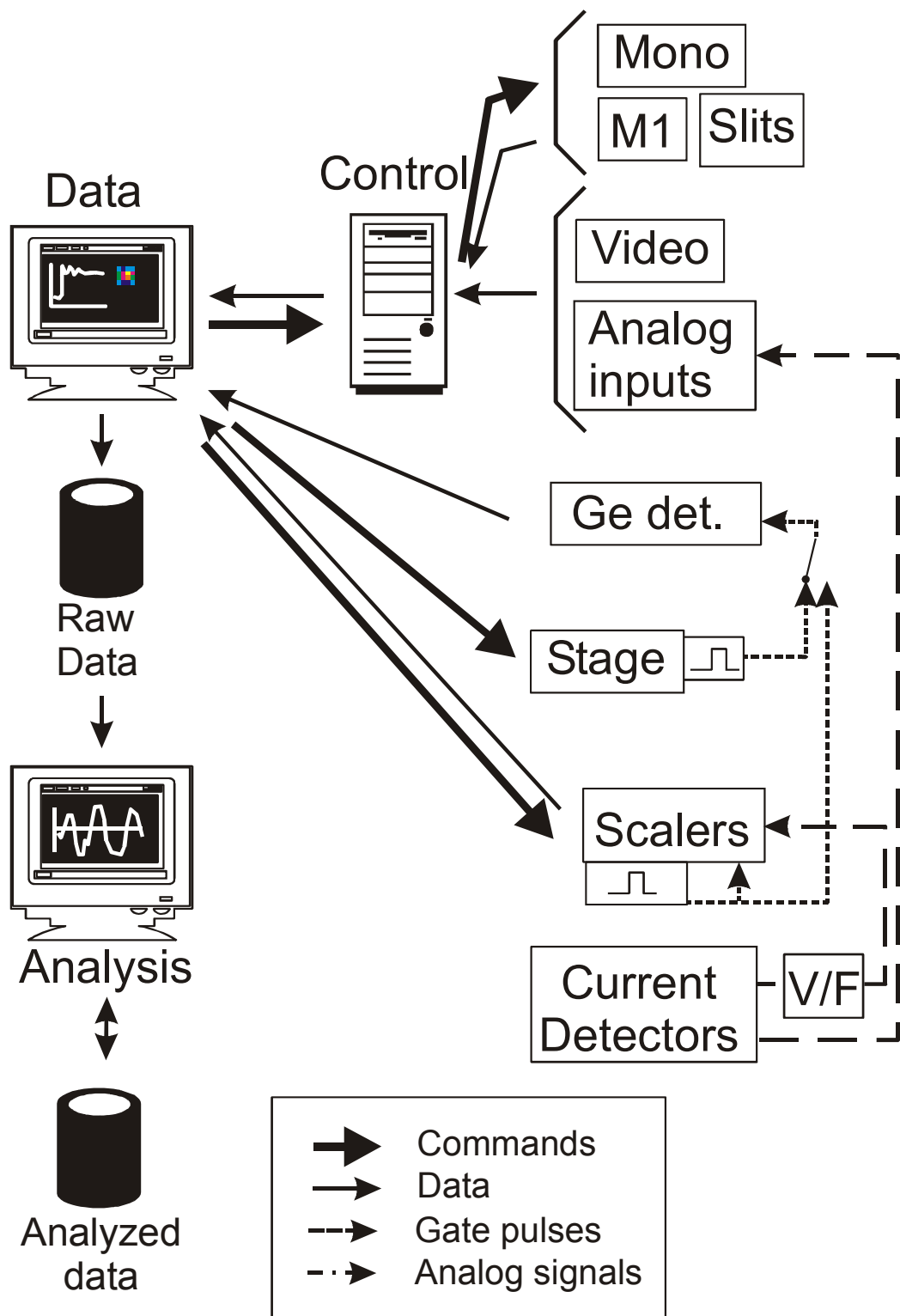


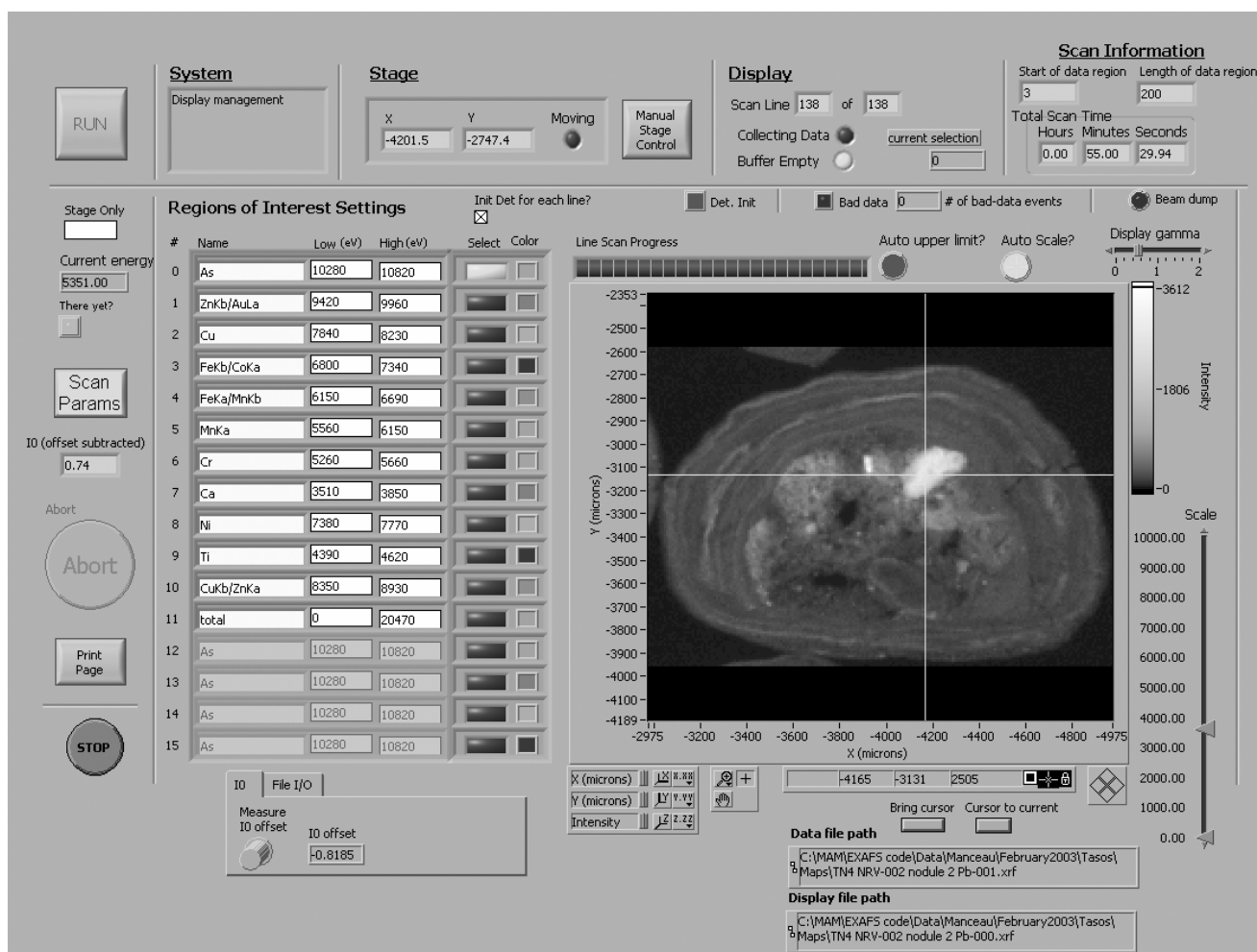


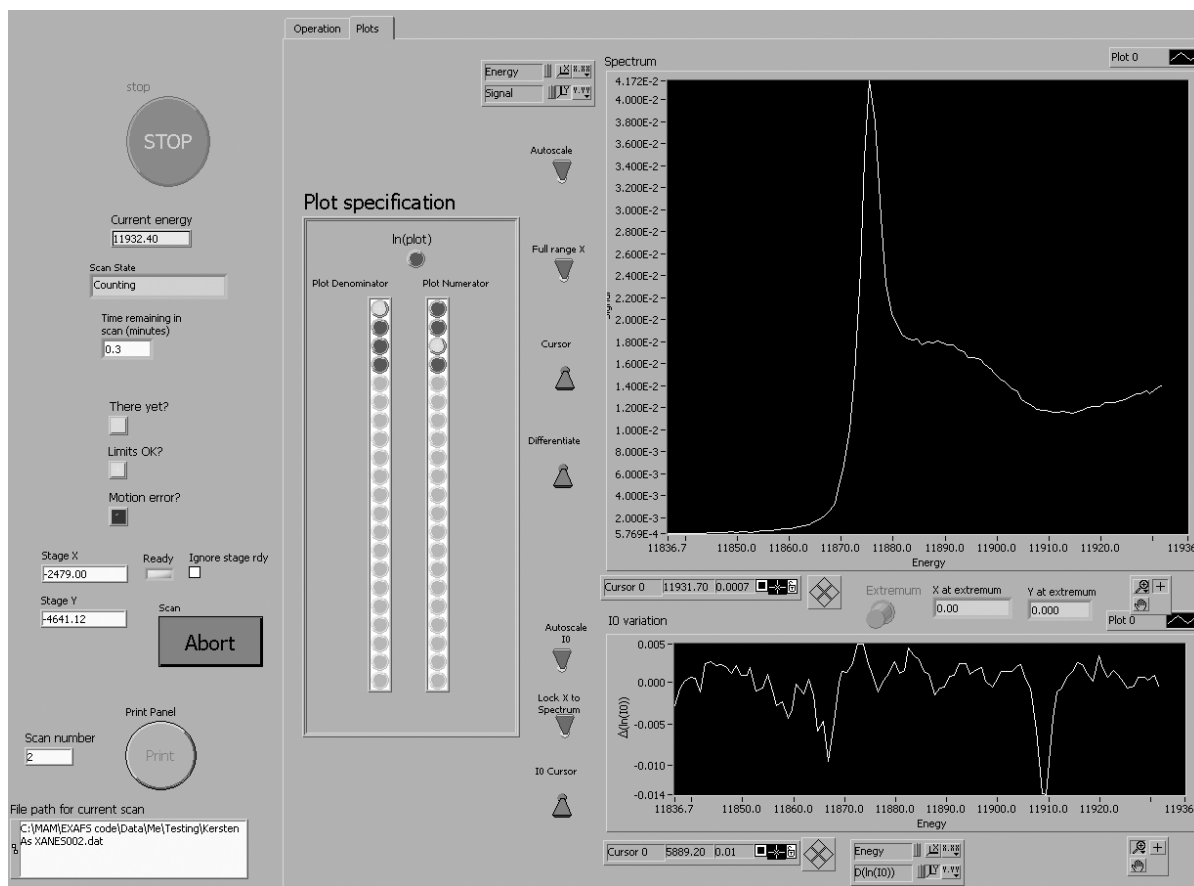


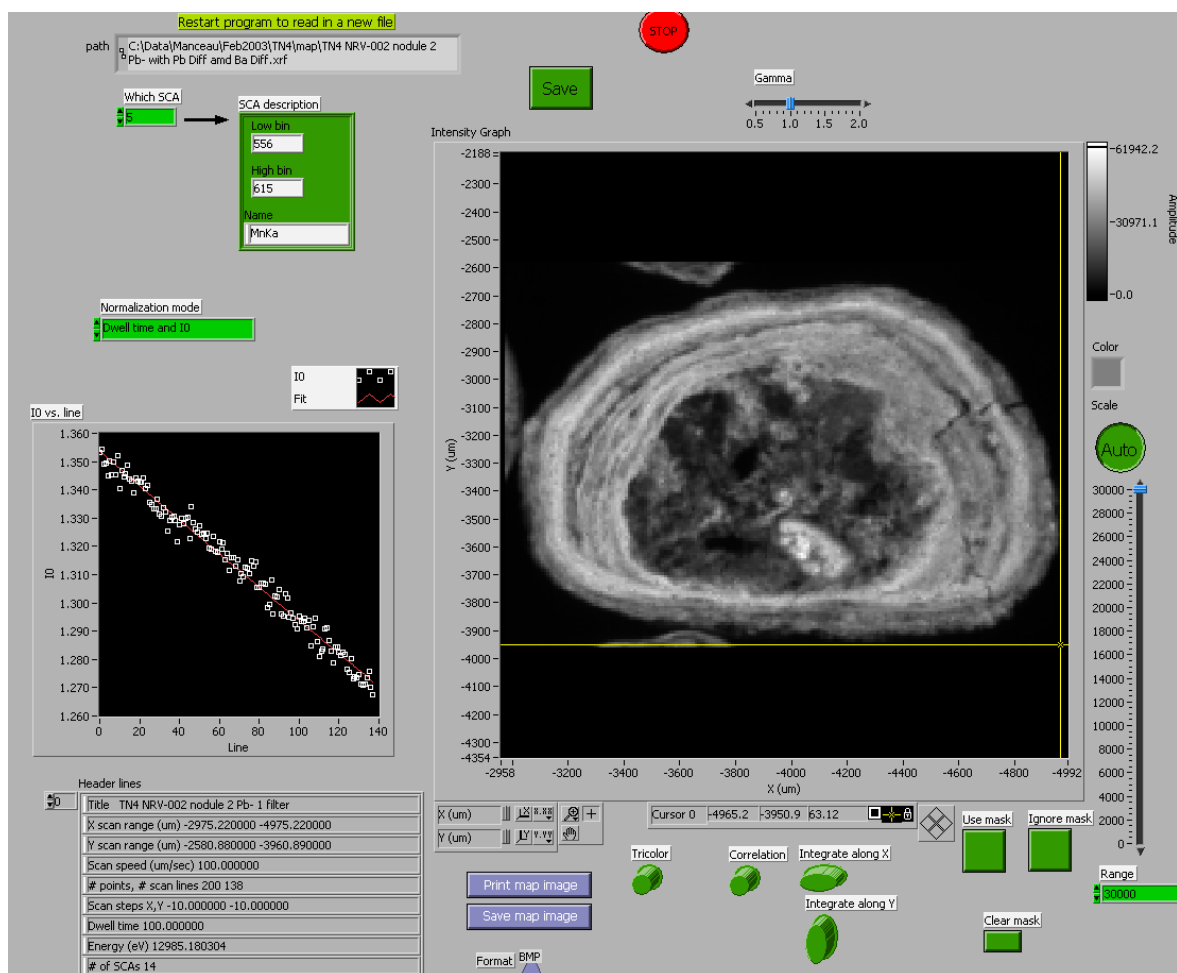


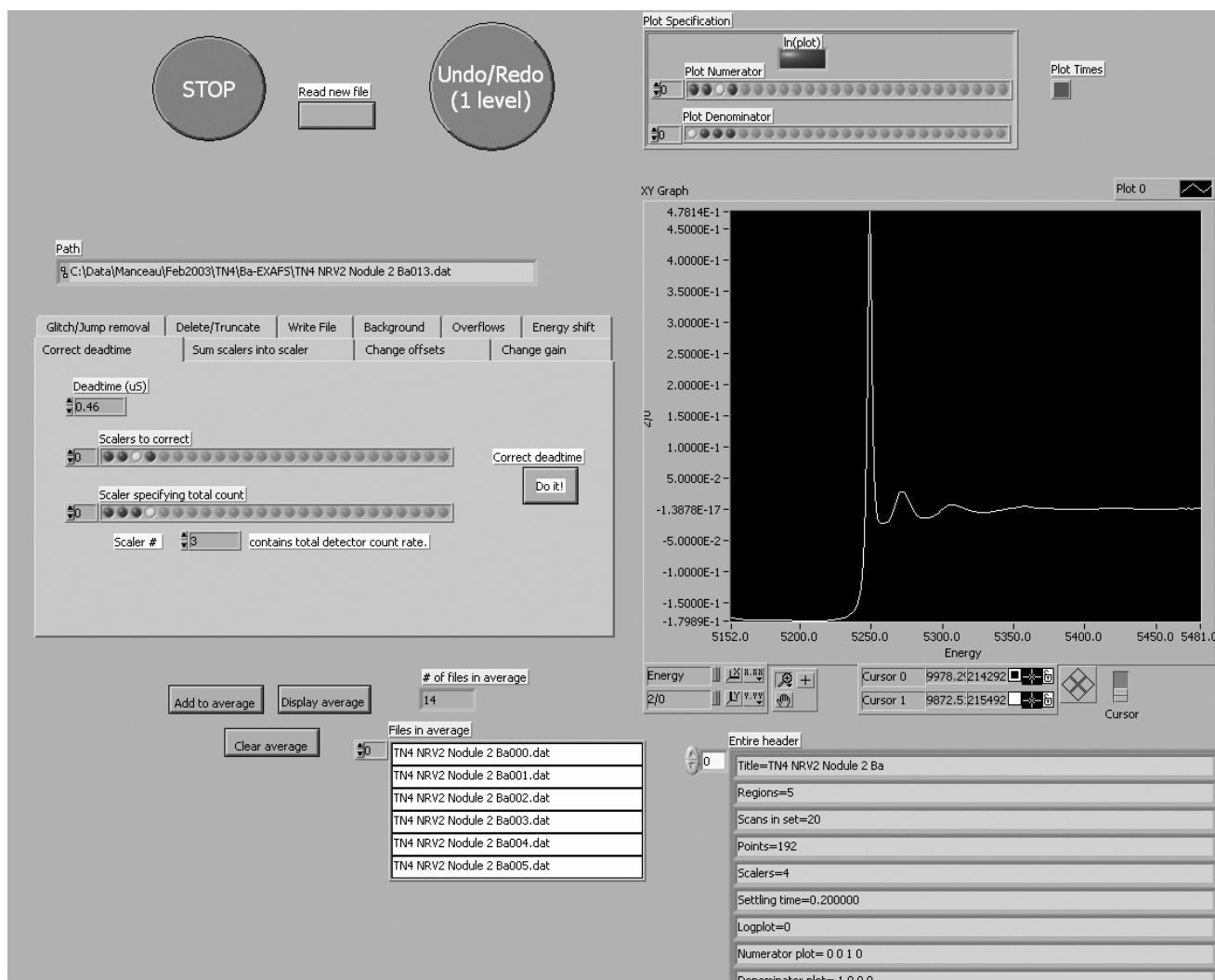


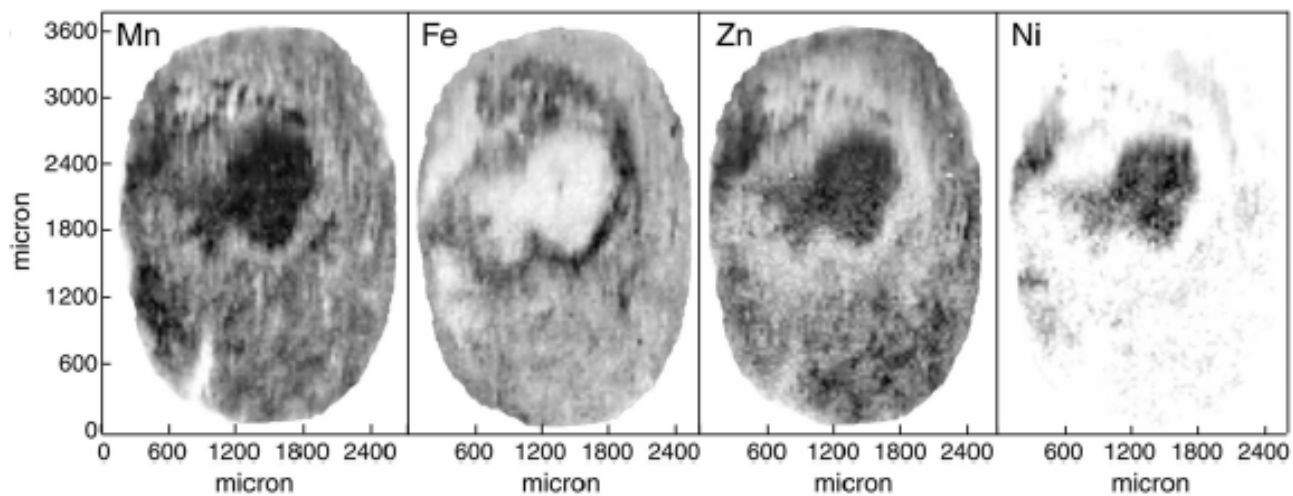












Goethite (4.19Å)

Birnessite (7.1Å)

Phyllosilicate (2.57Å)

Lithiophorite (9.4Å)

